This is the Pre-Published Version.

This is the Accepted Manuscript version of an article accepted for publication in ECS transactions. IOP Publishing Ltd is not responsible for any errors or omissions in this version of the manuscript or any version derived from it. The Version of Record is available online at https://doi.org/10.1149/07708.0027ecst.
This manuscript version is made available under the CC-BY-NC-ND 4.0 license (https://creativecommons.org/licenses/by-nc-nd/4.0/).

Solution Exfoliated Black Phosphorus and Its Applications

Shenghuang Lin and Shu Ping Lau*

Department of Applied Physics, The Hong Kong Polytechnic University,

Hong Kong SAR, P.R. China

Black phosphorus (BP), has recently attracted much attention all over the world and demonstrated great potential in novel nanoelectronics owing to its direct and narrow bandgap. Regarding to the scale production of BP and its related electronic devices, solution exfoliation reveals superior advances when compared with mechanical exfoliation. Remarkably, liquid-phase exfoliated BP flakes and quantum dots (QDs) exhibit exciting properties in solar cells, electronic, and optical devices. The exfoliation of BP in diverse solvents have been demonstrated. The solution exfoliated BP flakes can be an effective electron transport layer in organic photovoltaics (OPVs). The BP QDs can be incorporated in the active layer of OPV to enhance its power conversion efficiencies. In addition, the BP flakes exhibit nonlinear optical properties which can be an excellent saturable absorber for high energy pulse generation in fiber laser.

Due to their interesting properties, 2D (two-dimensional) materials have been explored carefully when thinned down to atomic layer scale and reveal significant changes in the mechanical, physical and chemical properties. For example, the bandgap of MoS_2, a typical member belonging to the family of transition metal dichalcogenides (TMDs), varies from 1.29 eV to 1.8 eV when the thickness of bulk was thinned down to single-layer [1], which ensures its great potential applications in photovoltaics [2-4], photodetectors [5, 6], and light emitters [7]. In addition to TMDs and graphene, scientists also pay much attention to explore new 2D semiconductors. Interestingly, the rediscovering of BP has excited materials scientists to make BP as a promising candidate for complementing graphene's deficiencies. Remarkably, both experimental and theoretical results revealed that BP possesses a direct bandgap ranging from 0.3 eV (bulk) to 2.0 eV (monolayer) [8], which can bridge the gap between zero-gap graphene and relatively large bandgap TMDs for infrared photonics and optoelectronics [9, 10]. Although room temperature hole mobilities of ~1000 $cm^2 \cdot V^{-1} \cdot s^{-1}$ with on/off ratios of ~10^3–10^5 can be achieved in mechanically exfoliated few-layer BP based field effect transistors (FETs) [11], such mechanical exfoliation technique suffers from low yield and a low production rate, which is not scalable for practical applications. As compared, solution-processed electronic devices are usually preferred due to its low cost, large area, flexibility and convenient materials integration [12-14]. Therefore, one possible solution is to exfoliate BP in liquid to give large scale dispersion of nanosheets to extend the application of BP. Here we demonstrated that BP flakes and BPQDs (black phosphorus quantum dots) can be effectively exfoliated from bulk BP by ultrasonication assisted solution process. The solution exfoliated BP flakes can be an

* Corresponding author: apsplau@polyu.edu.hk

effective electron transport layer in organic photovoltaics (OPVs). The BPQDs can be incorporated in the active layer of OPV to enhance its power conversion efficiencies. In addition, the BP flakes exhibit nonlinear optical properties which can be an excellent saturable absorber for high energy pulse generation in fiber laser.

Experimental

Preparation of BP flakes and BPQDs- BP crystals were purchased from Smart Elements. The solution-based mechanical exfoliation process started from the mixing of BP crystals with diverse solutions like IPA, NMP, acetone and ethanol, followed by sonication in an ultrasonic bath (400 W) at room temperature for 30 h. The resulted BP solution was purified by centrifugation, with a rate of 4000 rpm for 60 min, to remove larger particles. Then the residual BP dispersion was further turned into BPQDs by probe sonication again for 3 hrs. The final purified BP-solution mixture with an expected concentration can be obtained.

Characterizations- The microstructure of BP was studied on a scanning transmission electron microscope (TEM) (JEOL JEM-2100F, operated at 200 kV) and the TEM samples were prepared by drop-casting BP dispersion onto carbon grids.

Characterization of BP-Based Solar Cell- The J–V characteristics of the OPVs were measured by using a Keithley 2400 source meter under the illumination of 100 mW cm^{-2} (Newport 91160, 300 W, solar simulator equipped with an AM 1.5 filter). The light intensity was calibrated with a standard silicon solar cell. The external quantum efficiency (EQE) spectra of the devices were measured with a standard system equipped with a xenon lamp (Oriel 66902, 300W), a monochromator (Newport 66902), a Si detector (Oriel 76175_71580), and a dual channel power meter (Newport 2931_C).

Pump-Probe Measurement- The transient dynamical response measurements were performed using a femtosecond pulse laser with pulse duration of 35 fs and repetition rate of 2 kHz. Both the pump light and the probe light are at 1550 nm. The pump incident light power is 3.3×10^3 GW cm^{-2} and the probe incident light power is 0.5×10^3 GW cm^{-2}. The laser beam was focused by a lens with the focus distance of 250 mm. Any coherent artifact on the transient signal was eliminated by using the cross-polarized configuration. It was examined that the probe beam alone could not cause any nonlinear effect in our experiments.

Results and discussion

As we mentioned, ultrasonication method was employed to exfoliate bulk BP crystals into ultrathin flakes and QDs. The schematic illustrations of ultrasonication process is shown in Figure 1. Firstly, BP crystal was placed into the target solution and ground for several minutes. Then the mixture was sonicated for 30h and the resulted BP solution was purified to get supernatant liquid. After that the supernatant liquid was drop-casted onto TEM grid for observation. The obtained BP flakes and BPQDs can be found in Figure 1, which is similar to the results reported in Refs. [13, 15, 16]. The obtained sizes of BP flakes and BPQDs in this work are in the range of 50 nm – 1 μm and 2 -10 nm, respectively.

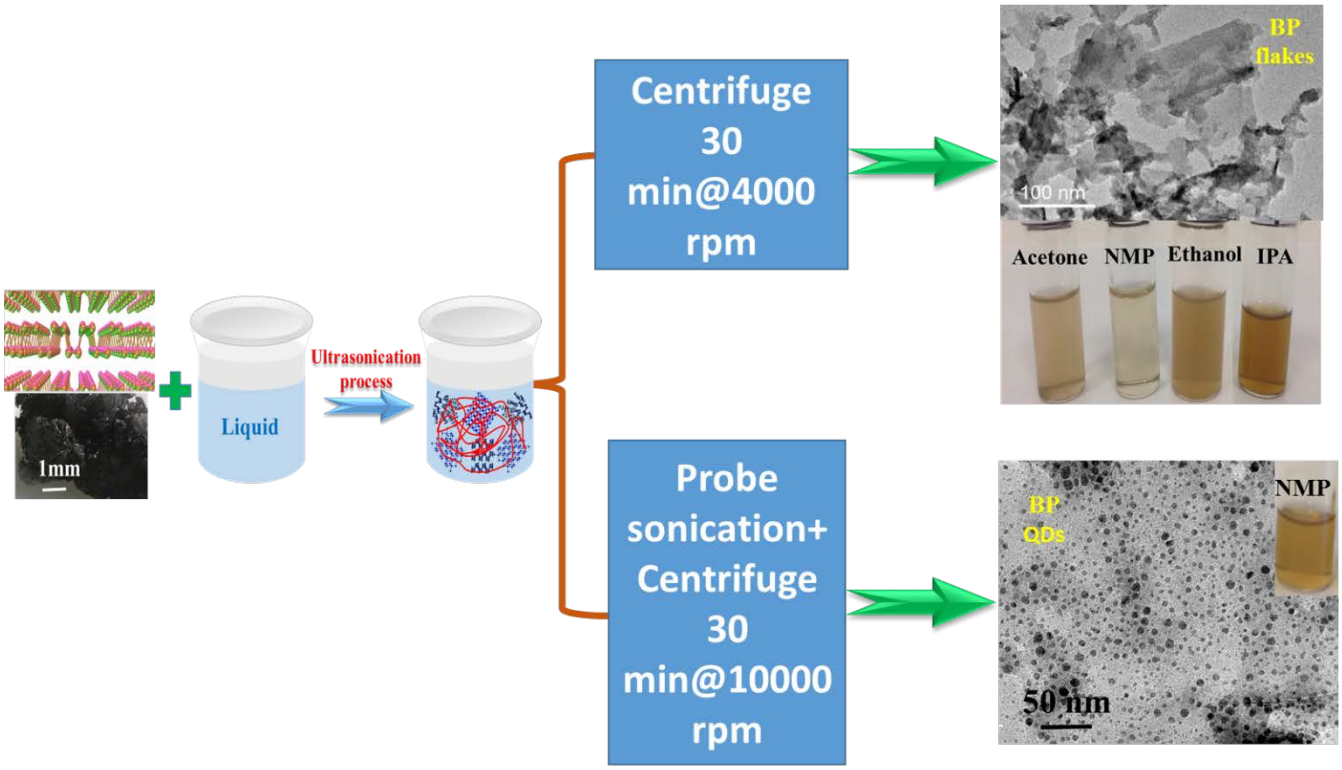

Figure.1 Molecular structure and photograph of black phosphorus crystal. Illustrations of the ultrasonication process of BP flakes and BPQDs as presented above. It also showed the photographs of the exfoliated BP flakes and BPQDs in acetone, IPA, ethanol, and NMP solvents.

Next, we demonstrate the utilization of the solution exfoliated BP in OPVs as carrier-transport layers, including ETL (electron transport layer) and HTL (hole transport layer). As the low concentration of solution processed BP flakes cannot make full coverage on a substrate due to the poor conductivity of spin-coated BP films, it is difficult to utilize individual BP as a carrier-transport layer. Therefore, we introduced BP onto PEDOT:PSS and ZnO layers to change the hole and electron transport behavior in OPVs, respectively. Here we fabricated two types of OPV devices with conventional and inverted structures as shown in Figure 2a. Poly[4,8-bis[(2-ethylhexyl)oxy]benzo[1,2-b:4,5-b']dithiophene-2,6-diyl][3-fluoro-2-[(2-ethylhexyl)carbonyl]thieno[3,4-b]-thiophenediyl] (PTB7), and [6,6]-phenyl-C71-butyric-acid-methyl-ester ($PC_{71}BM$) were used as the p-type and n-type active layer materials, respectively. It is crucial to control the thickness of BP deposited on the ETL/HTL to optimize its enhancement in charge transfer, which is realized by spin coating BP-ethanol solution for different times. The ethanol solution is chosen because of its compatibility with PEDOT:PSS and ZnO films. The current density–voltage (J–V) characteristics of the two types of OPVs with the incorporation of BP are shown in Figure 2b,c In terms of conventional structure, BP incorporated onto PEDOT:PSS as HTL gives rise to the decrease of the short-circuit current density (Jsc) and open-circuit voltage (Voc), resulting in the degradation of power conversion efficiencies (PCE) of the devices. However, when BP is employed onto ZnO as the ETL in the inverted device, we can observe the obvious improvement of Jsc and PCE, as depicted in Figure 2c. Namely, the power conversion efficiencies (PCEs) of the BP-incorporated OPVs can be improved to 8.18% in average with the relative enhancement of 11%. The incorporation of BP flakes with the optimum thickness of $\approx$10 nm can form cascaded band structure in OPVs, which can facilitate electron transport and enhance the PCEs of the devices.

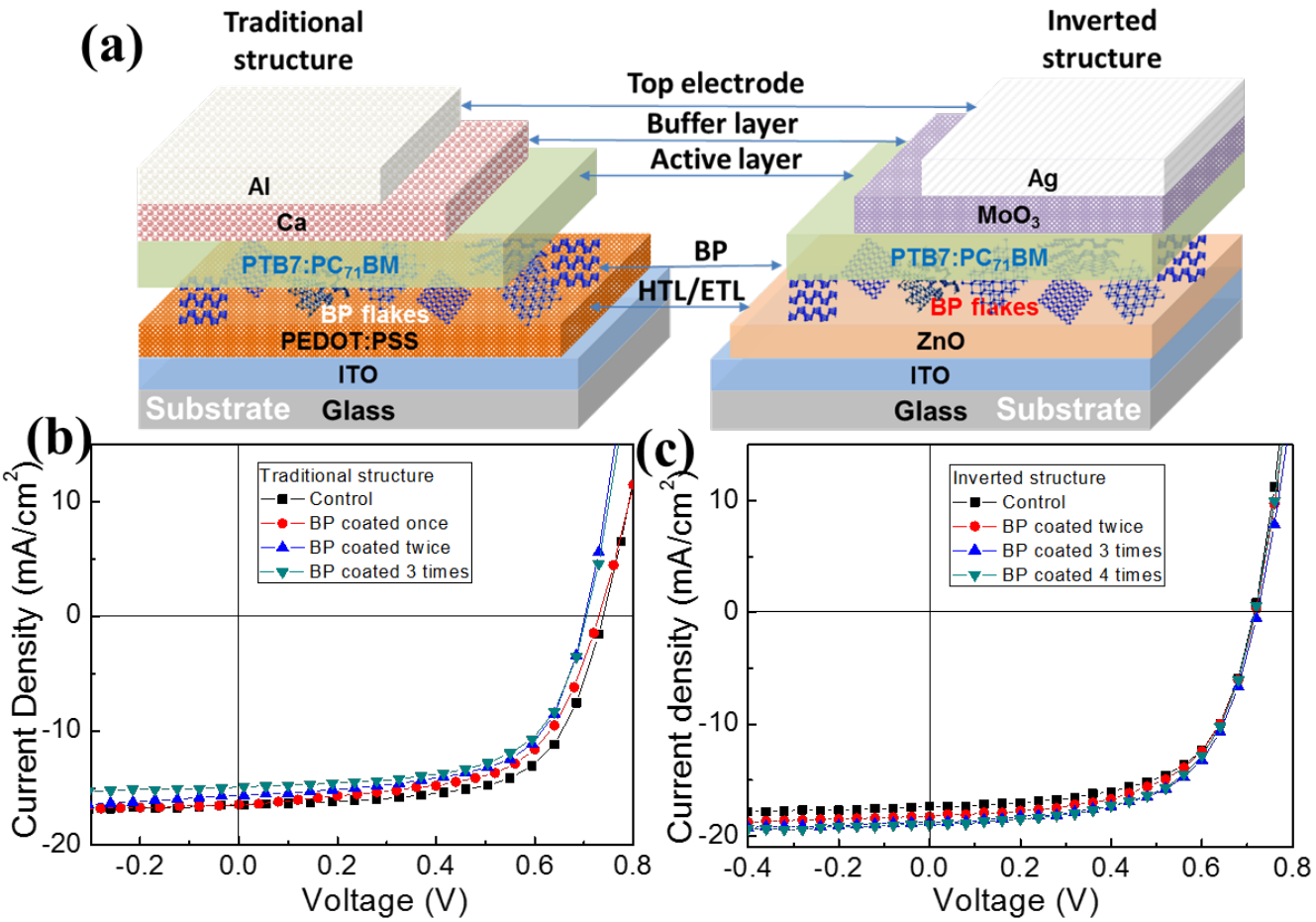

Figure.2 (a) Conventional and inverted architectures of OPVs based on PTB7:$PC_{71}BM$; J–V characteristics of (b) conventional, and (c) inverted OPVs with BP incorporation under different conditions.

OPVs with incorporation of BPQDs into the device structure is also demonstrated and shown in Figure 3a. The samples were fabricated by solution process on indium tin oxide (ITO) glass, in which BPQDs were added in the active layer only for low percentage. We first fabricated the OPV devices based on PTB7:$PC_{71}BM$ with addition of BPQDs. The representative current density-voltage (J-V) characteristics of the OPVs with introduction of BPQDs with different percentage (0.5, 1.0, 3.0 vol.%) is shown in Figure 3b. The size of the added BPQDs is estimated to be ~4.50 ± 0.88 nm. Inset in Figure 3b reveals the corresponding energy diagram of the device. All of the energy levels of PTB7: $PC_{71}BM$ were chosen from the literature [17]. Cascaded band structure can be formed when incorporating BPQDs into the device, which is favorable for efficient carrier transport and can prohibit carrier recombination. The PTB7:$PC_{71}BM$ control devices give an average Voc of 0.713 V, Jsc of 16.59 mA/cm^2, FF of 65.1% and an average PCE of 7.70%. With addition of 0.5 and 1.0 vol.% BPQDs into the photoactive layer, the Voc and FF of the devices stayed almost constant, while the average Jsc increased significantly to 17.66 and 18.07 mA/cm^2, respectively. As a result, PCE of the OPVs improved to 8.21% and 8.60% on average with incorporation of 0.5% and 1.0 vol.% BPQDs, respectively. However, with further increase of the concentration of BPQDs to 3 vol.%, the performance of OPVs decreased with average PCE of 8.11% due to the decrease of both Jsc and FF of the devices. The champion device obtained with incorporation of 1.0 vol.% BPQDs shows the Voc, Jsc, and FF of 0.715 V, 18.12 mA/cm^2, and 67.2%, respectively, which leads to a best PCE of 8.71% with relatively 13.1% PCE enhancement compared to the control devices. EQE measurements of the OPVs were subsequently conducted to better illuminate the enhancement of the device performance, as shown in Figure 3c. It is clear to observe that the improvement of EQE can be

found in the whole characterized wavelength range. In particularly, the control device without BPQDs exhibits the maximum EQE of 78.41%, while the others added with 0.5 vol.% and 1 vol.% BPQDs gives the maximum EQEs of 83.21% and 84.63%, respectively.

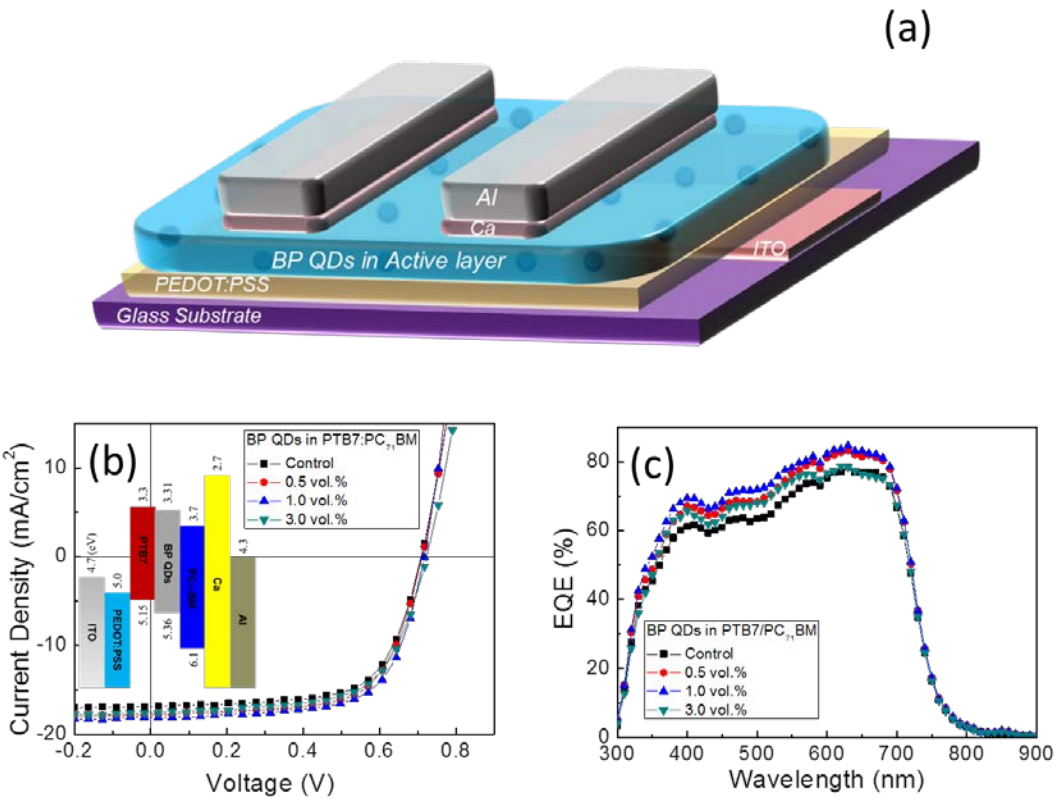

Figure.3 (a) Device architecture of the OPVs with the incorporation of BPQDs in bulk heterojunction active layer. (b) Current density-voltage (J-V) and (c) EQE characteristics of the best control device and the OPVs with various addition levels (0.5, 1.0, 3.0 vol.%) of BPQDs (D = 4.5 nm).

Moreover, we also measured the nonlinear property of BP. Similar to the graphene-polymer composite [18], BP-PVP composite film can be easily transferred and attached onto the end-facet of optical fiber ferrule. As shown in Figure 4b, BP-covered optical fiber is then incorporated into the fiber laser cavity. In a standard operation, we first excluded the possibility of self-Q-switching of the fiber laser. Without using the BP device, only continuous wave (CW) emission was obtained even when we increased the pump power from the start oscillation threshold to the maximum and/or tuned the angle of polarization from 0° to 360° by adjusting the polarization controllers (PCs). After inserting the BP saturable absorber device, Q-switching state occurred at an incident pump power of only 25 mW, which is a very low threshold value in comparison to those of graphene [19, 20] and TMDs-based saturable absorbers. The results of pulse generation with BP-PVP saturable absorber at the pump power of 140 mW are shown in Figure 4c–f. Typical Q-switching output spectrum is shown in Figure 4c. It can be seen that the fiber laser operated with the central wavelength of 1561.9 nm. Its 3 dB bandwidth is 1.5 nm. Figure 4d shows the typical pulse train with uniform intensity distribution which reveals a repetition rate of 23.48 kHz, corresponding to a time interval of 42.5 μs. The intensity distribution is very uniform without modulation, indicating good noise suppressing capability of BP-PVP composite. Figure 4e is the corresponding single pulse profile in time domain with a narrower sweep span. The pulse has a full width at half maximum (FWHM) of 4.35 μs with symmetric intensity profile. We have measured the radio-frequency (RF) spectrum (Figure 4f) and found that the signal-to-noise ratio is over 53 dB, indicating high quality of the output pulse. In addition, apart from the fundamental and harmonic frequency, we did not observe other frequency component in

the RF spectrum with wider span (see inset of Figure 4f), confirming high stability of the Q-switched pulse generation.

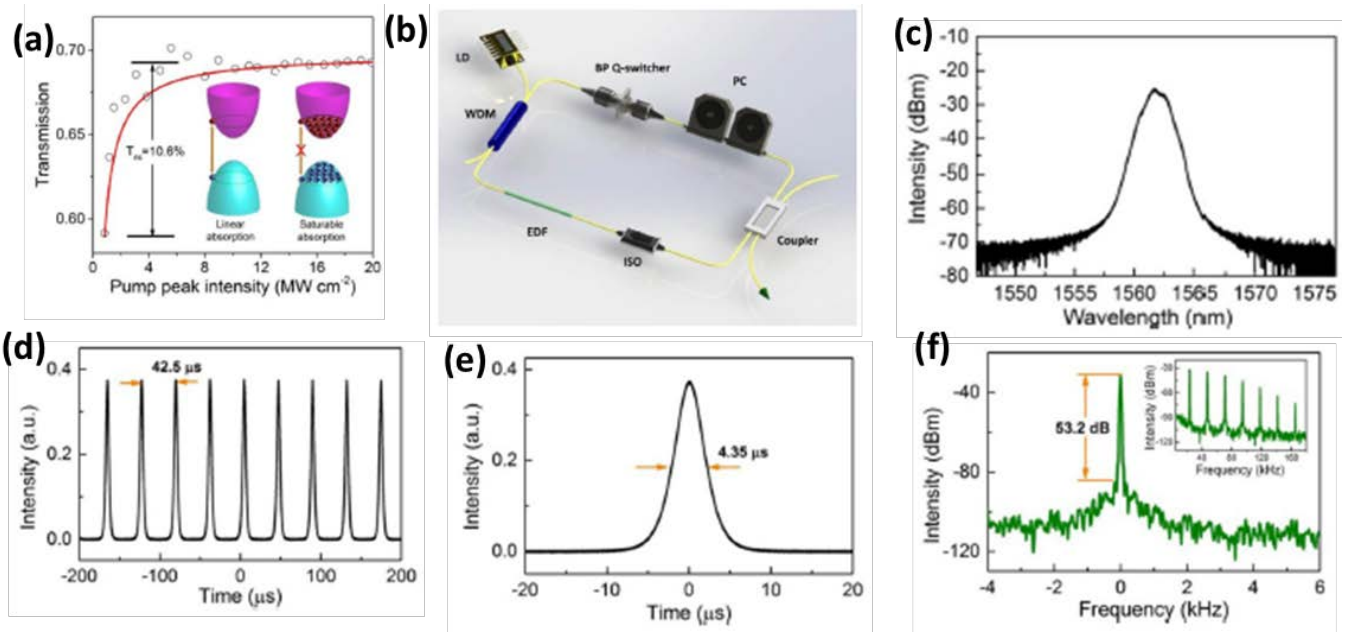

Figure.4 (a) The collected saturable absorption curve of BP-polymer composites measured at 1565 nm. The insets show the energy diagrams of the saturable absorption and linear absorption. (b) Schematic illustration of the ring cavity of the utilized Q-switched fiber laser, where LD, ISO, WDM, PC and EDF respectively represent 974 nm laser diode, polarization-independent isolator, wavelength division multiplexer, polarization controller and erbium-doped fiber. (c) Optical spectrum of the Q-switching. (d) Q-switching pulse train of the Q-switching. (e) Single Q-switching pulse. (f) The obtained radiofrequency optical spectrum at the fundamental frequency and the wideband RF spectrum (inset).

Conclusions

In summary, the solution-exfoliated BP flakes and BPQDs are demonstrated. The solution exfoliated BP flakes can be utilized as ETL in OPVs and the average PCE of the OPVs is enhanced by 11% relatively when compared to that of the control device, corresponding to the increase of PCE from 7.37% to 8.18%. BPQDs can also be incorporated into the active layer of OPVs and the efficiencies of the devices are substantially enhanced. Moreover, BP flakes reveal very fast carrier dynamics and BP-polymer composite has a modulation depth of 10.6%. The incorporation of BP nanoflakes into polymer matrix not only protects BP from ambient environments but also produces a new type of optical material by combining the special optical properties of BP with the structural properties of the polymer. Generally, solution-processible BP can widely extend its applications in the fields of photonics and optoelectronics.

Acknowledgements

This work was financially supported by the PolyU grants (1-BBAD and 1-ZVGH) and the Research Grants Council (RGC) of Hong Kong (Project no. PolyU 153271/16P).

References

[1] K. F. Mak, C. Lee, J. Hone, J. Shan, T. F. Heinz, *Phys. Rev. Lett.*, 105, 136805 (2010).
[2] J. Feng, X. F. Qian, C. W. Huang, J. Li, *Nat. Photonics*, 6, 866-872 (2012).
[3] M. Fontana, T. Deppe, A. K. Boyd, M. Rinzan, A. Y. Liu, M. Paranjape, P. Barbara, *Sci. Rep.*, 3, 1634 (2013).

[4] M. Bernardi, M. Palummo, J. C. Grossman, *Nano Lett.*, 13, 3664-3670 (2013).
[5] Z. Y. Yin, H. Li, H, Li, L. Jiang, Y. Shi, Y. Sun, G. Lu, Q. Zhang, X. Chen, H. Zhang, *ACS Nano*, 6, 74-80 (2011).
[6] H. S. Lee, S. W. Min, Y. Chang, M. K. Park, T. Nam, H. Kim, J. Kim, S. Ryu, S. Im, *Nano Lett.*, 12, 3695-3700 (2012).
[7] Y. Ye, Z. Ye, M. Gharghi, H. Zhu, M. Zhao, X. Yin, X. Zhang, *arXiv*, 1305, 4235 (2013).
[8] L. Li, Y. Yu, G.J. Ye, Q. Ge, X. Ou, H. Wu, D. Feng, X.H. Chen, Y. Zhang, *Nat. Nano.*, 9, 372-377 (2014).
[9] A.S. Rodin, A. Carvalho, A.H. Castro Neto, *Phys. Rev. Lett.*, 112, 176801 (2014).
[10] S. Das, W. Zhang, M. Demarteau, A. Hoffmann, M. Dubey, A. Roelofs, *Nano Lett.*, 14, 5733-5739 (2014).
[11] H. Liu, Y. Du, Y. Deng, P.D. Ye, *Chem. Soc. Rev.*, 44, 2732-2743 (2015).
[12] G. Konstantatos, I. Howard, A. Fischer, S. Hoogland, J. Clifford, E. Klem, L. Levina, E.H. Sargent, *Nature*, 442, 180-183 (2006).
[13] S. Lin, S. Liu, Z. Yang, Y. Li, T.W. Ng, Z. Xu, Q. Bao, J. Hao, C.-S. Lee, C. Surya, F. Yan, S.P. Lau, *Adv. Func. Mater.*, 26, 864-871 (2016).
[14] S. Lin, Y. Li, W. Lu, Y. Chui, L. Rogée, Q. Bao, S. Lau, *2D Mater.*, 4, 025001 (2017).
[15] H. Mu, S. Lin, Z. Wang, S. Xiao, P. Li, Y. Chen, H. Zhang, H. Bao, S.P. Lau, C. Pan, D. Fan, Q. Bao, *Advanced Optical Materials*, 3, 1447-1453 (2015).
[16] X. Zhang, H. Xie, Z. Liu, C. Tan, Z. Luo, H. Li, J. Lin, L. Sun, W. Chen, Z. Xu, L. Xie, W. Huang, H. Zhang, *Angew. Chem. Int. Ed.*, 54, 3653-3657 (2015).
[17] S. Liu, P. You, J. Li, J. Li, C.-S. Lee, B. S. Ong, C. Surya, F. Yan, *Energy & Environmental Science*, 8, 1463 (2015).
[18] Q. Bao, H. Zhang, J. X. Yang, S. Wang, D. Y. Tang, R. Jose, S. Ramakrishna, C. T. Lim, K. P. Loh, *Adv. Funct. Mater.*, 20, 782 (2010).
[19] D. Popa, Z. Sun, T. Hasan, F. Torrisi, F. Wang, A. C. Ferrari, *Appl. Phys. Lett.*, 98, 073106 (2011).
[20] W. Cao, H. Wang, A. Luo, Z. Luo, W. Xu, *Laser Phys. Lett.*, 9, 54 (2012).